RESEARCH ARTICLE

Magnetic Resonance in Medicine

Wideband black-blood late gadolinium enhancement imaging for improved myocardial scar assessment in patients with cardiac implantable electronic devices

Pauline Gut[1,2] | Hubert Cochet[1,3] | Guido Caluori[1] | Dounia El-Hamrani[1] | Marion Constantin[1] | Konstantinos Vlachos[1] | Soumaya Sridi[3] | Panagiotis Antiochos[2] | Jürg Schwitter[2] | Ambra Masi[2] | Frederic Sacher[1,4] | Pierre Jaïs[1,4] | Matthias Stuber[1,2,5] | Aurélien Bustin[1,2,3,6]

[1]IHU LIRYC, Electrophysiology and Heart Modeling Institute, Université de Bordeaux, INSERM, CRCTB, U 1045, IHU Liryc, Bordeaux, France

[2]Department of Diagnostic and Interventional Radiology, Lausanne University Hospital and University of Lausanne, Lausanne, Switzerland

[3]Department of Cardiovascular Imaging, Hôpital Cardiologique du Haut-Lévêque, CHU de Bordeaux, Pessac, France

[4]Department of Cardiac Pacing and Electrophysiology, Hôpital Cardiologique du Haut-Lévêque, CHU de Bordeaux, Pessac, France

[5]CIBM Center for Biomedical Imaging, Lausanne, Switzerland

[6]Hôpital Xavier Arnozan, Pessac, France

Correspondence
Aurélien Bustin, IHU LIRYC, Electrophysiology and Heart Modeling Institute, Université de Bordeaux – INSERM U1045, Avenue du Haut Lévêque, 33604, Pessac, France.
Email: aurelien.bustin@ihu-liryc.fr

Abstract

Purpose: Wideband phase-sensitive inversion recovery (PSIR) late gadolinium enhancement (LGE) enables myocardial scar imaging in implantable cardioverter defibrillators (ICD) patients, mitigating hyperintensity artifacts. To address subendocardial scar visibility challenges, a 2D breath-hold single-shot electrocardiography-triggered black-blood (BB) LGE sequence was integrated with wideband imaging, enhancing scar-blood contrast.

Methods: Wideband BB, with increased bandwidth in the inversion pulse (0.8–3.8 kHz) and T_2 preparation refocusing pulses (1.6–5.0 kHz), was compared with conventional and wideband PSIR, and conventional BB, in a phantom and sheep with and without ICD, and in six patients with cardiac devices and known myocardial injury. ICD artifact extent was quantified in the phantom and specific absorption rate (SAR) was reported for each sequence. Image contrast ratios were analyzed in both phantom and animal experiments. Expert radiologists assessed image quality, artifact severity, and scar segments in patients and sheep. Additionally, histology was performed on the sheep's heart.

Results: In the phantom, wideband BB reduced ICD artifacts by 62% compared to conventional BB while substantially improving scar-blood contrast, but with a SAR more than 24 times that of wideband PSIR. Similarly, the animal study demonstrated a considerable increase in scar-blood contrast with wideband BB, with superior scar detection compared with wideband PSIR, the latter confirmed by histology. In alignment with the animal study, wideband BB successfully eliminated severe ICD hyperintensity artifacts in all patients, surpassing wideband PSIR in image quality and scar detection.

Conclusion: Wideband BB may play a crucial role in imaging ICD patients, offering images with reduced ICD artifacts and enhanced scar detection.

KEYWORDS
black-blood LGE imaging, cardiac implantable electronic device, implantable cardioverter defibrillator, myocardial scar LGE imaging, susceptibility artifacts, wideband LGE imaging

1 | INTRODUCTION

Sudden cardiac death is a leading cause of mortality,[1,2] primarily attributed to ventricular tachycardia (VT). Individuals suffering from VT are usually treated with implantable cardioverter defibrillators (ICDs) and pacemakers, with ~1.7 million implantations occurring worldwide each year.[3] Assessment of myocardial scars in patients with cardiac devices is essential to better understand the underlying structural abnormalities of the heart and to adapt therapeutic strategies accordingly.

Although bright-blood late gadolinium enhancement (LGE) imaging with ICD can be safely performed at 1.5 T for patients who are not device-dependent,[4–7] severe hyperintensity artifacts caused by the metallic device compromise the image and limit its interpretation and diagnosis.[8–10] Rashid et al.[11] introduced the concept of wideband phase-sensitive inversion recovery (PSIR) LGE by increasing the spectral bandwidth of the inversion recovery pulse to 3.8 kHz to reduce ICD hyperintensity artifacts. Unfortunately, and although very efficient, conventional, and wideband PSIR-LGE still suffer from poor contrast at the scar-blood interface, making them particularly challenging to depict subendocardial scars.

Several approaches have been proposed to improve scar-blood contrast, such as the use of a double inversion[12] or a T_2 magnetization-preparation module.[13,14] Although these techniques improve scar-blood contrast, the scar-myocardium contrast is reduced. Alternatively, dark-blood LGE imaging[15,16] has been developed to improve scar-blood contrast without losing scar-myocardium contrast. Combining magnetization-preparation with inversion recovery, the normal myocardium null time point can be shifted relative to blood by choosing the correct TI so that healthy myocardial and blood signals can be nulled simultaneously while enhancing scar tissue. Several studies have investigated different strategies to achieve LGE with simultaneous suppression of blood and normal myocardium signals,[15–22] but none of these techniques has been combined with wideband imaging and tested in patients with CIED.

In this work, a black-blood LGE imaging sequence was combined with a wideband inversion pulse and a wideband T_2 preparation to both improve myocardial scar visualization in ICD patients and to reduce potential ICD-induced image artifacts. The objective of this study was to assess the feasibility of wideband black-blood LGE imaging for enhanced scar detection in phantom, animal, and patient studies with ICD at 1.5 T.

2 | METHODS

This study was approved by the Biomedical Research Ethics Committee and conformed to the Declaration of Helsinki. All patients provided informed consent for participation in this study. The animal study was carried out in accordance with the recommendations of the European Union (2010/63/EU) for the care and use of laboratory animals and conformed to the ethical guidelines of the French Ministry of Agriculture and Forests (Animal Health and Protection Veterinary Service). The protocol was approved by the local ethics committee "CE050" (APAFIS 39509).

2.1 | 2D wideband black-blood LGE sequence

A 2D breath-hold single-shot electrocardiography (ECG)-triggered gradient echo readout (GRE) wideband black-blood (BB) LGE sequence was implemented (Figure 1A). BB images were generated during odd heartbeats by a non-selective adiabatic hyperbolic secant (HS) 180° inversion recovery (IR) pulse (duration = 10.24 ms) followed by an adiabatic T_2 preparation[14] (T_2prep, duration of TE = 27 ms). The adiabatic T_2prep, relatively insensitive to B_1 and B_0 field inhomogeneities, consisted of a 90° tip-down pulse, of two adiabatic HS refocusing pulses (duration = 12.8 ms), and of a 90° tip-up pulse. A spoiling gradient was then applied to remove any residual transverse magnetization. For each slice, at least four single-shot images were acquired during mid-diastole, with an empty heartbeat in between to allow magnetization recovery, and were then averaged.

To eliminate the hyperintensity artifacts from the non-properly inverted myocardium signal in the presence of ICD, the HS IR spectral bandwidth was increased from 0.8 to 3.8 kHz[12] ($\mu = 16$, $\beta = 750$ rad/s), with a peak B_1 amplitude of 19 μT, in both PSIR and BB, hereafter, referred to as wideband PSIR and wideband BB, respectively (Figure 1B).

To further reduce ICD artifacts, the spectral bandwidth of the two T_2prep refocusing pulses in the wideband BB sequence was increased from 1.6 to 5.0 kHz ($\mu = 25$, $\beta = 785$ rad/s; originally created for a pulse duration of 10.24 ms, yielding a bandwidth of 6.2 kHz), with a peak B_1 amplitude of 30 μT (Figure 1B). The wideband T_2prep refocusing bandwidth was designed with Bloch simulations and optimized in previous phantom studies. Starting with the bandwidth of the conventional refocusing pulse in the T_2prep module, an iterative approach was adopted by creating several T_2prep refocusing pulses with progressively wider spectral bandwidths, while maintaining a fixed pulse duration of 10.24 ms, and optimizing various

FIGURE 1 Framework. (A) Pulse sequence design: 2D breath-hold single-shot electrocardiography (ECG)-triggered GRE BB imaging. BB LGE images were acquired during odd heartbeats with a non-selective adiabatic hyperbolic secant 180° IR followed by an adiabatic T_2prep module. A GRE readout was then applied. (B) Left: Inversion profile of the IR pulse. Conventional IR bandwidth = 0.8 kHz, wideband IR bandwidth = 3.8 kHz. Right: Inversion profile of the T_2 prep refocusing pulses. Conventional T_2prep refocusing bandwidth = 1.6 kHz, wideband T_2prep refocusing bandwidth = 5.0 kHz. BB, black-blood; GRE, gradient echo; IR, inversion recovery; LGE, late gadolinium enhancement; Mz/M0, normalized longitudinal magnetization; T_2prep, T_2 preparation.
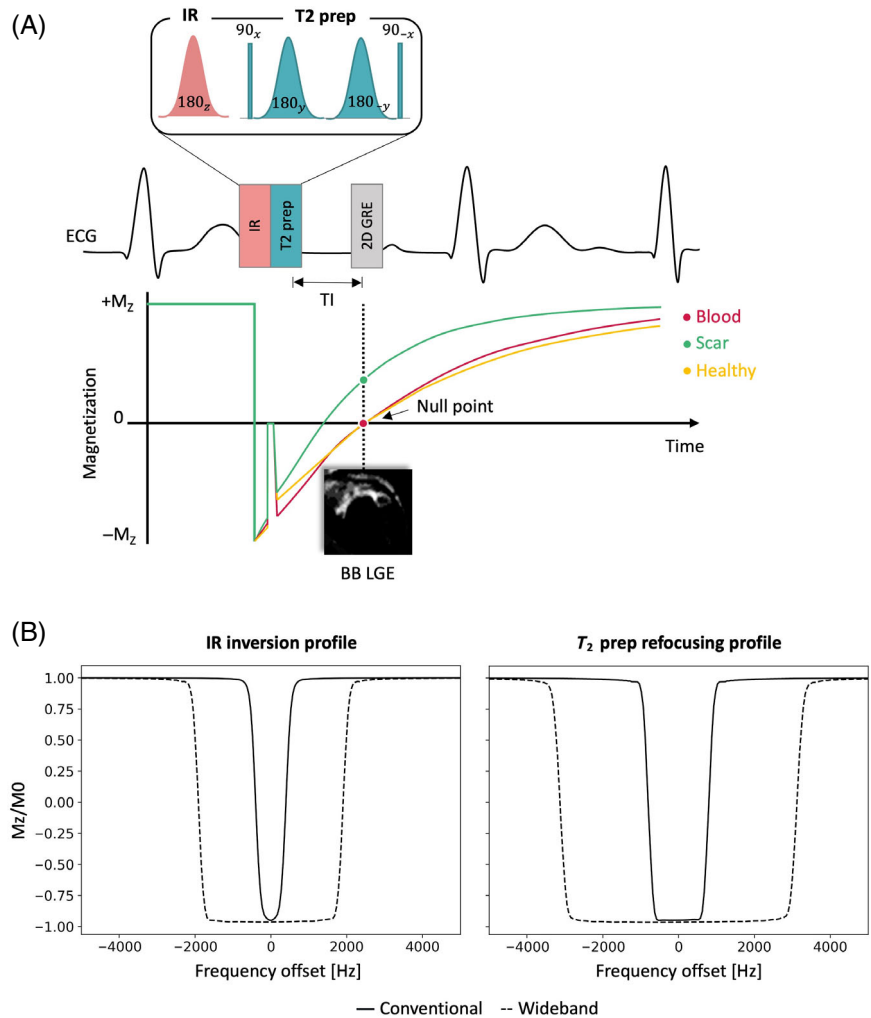
parameters such as μ and β through Bloch simulations. The pulses were then integrated into the T_2prep module of the BB sequence and tested in a phantom with an ICD, while maintaining a fixed IR bandwidth of 3.8 kHz.[11] Starting with the conventional T_2prep refocusing bandwidth of 1.6 kHz, the different T_2 preparation pulses were applied one after the other, with progressively increasing bandwidth, until a sufficiently wide bandwidth was found to satisfactorily reduce hyperintensity artifacts. The T_2prep refocusing pulses with a bandwidth of 5.0 kHz were identified as the optimal choice.

Finally, to eliminate bSSFP-associated ripple artifacts in the presence of ICD, GRE was used for conventional and wideband PSIR,[23] and for conventional and wideband BB.

2.2 | Phantom study

A phantom study was carried out on a 1.5 T system (MAG-NETOM Aera) using the T1MES phantom,[24,25] which contained nine differently doped tubes with agarose gel covering T_1 and T_2 ranges mimicking those of myocardium and blood, pre- and post-gadolinium-based contrast, at 1.5 T and 3 T. Conventional and wideband versions of PSIR and BB were tested in the phantom with and without an ICD. In case of ICD, the ICD (St. Jude, Quadra Assura CD3367-40Q) was taped to the side of the phantom at 4 cm, with a cushion in between (Figure 2A).

Sequence parameters are reported in Table 1. The optimal TIs for conventional and wideband PSIR were determined with a conventional and wideband PSIR TI scout, respectively, and the optimal TIs for conventional and wideband BB were determined with a conventional and wideband BB TI scout, respectively. An ECG was simulated with a heart rate of 60 bpm.

2.3 | Animal study

Cardiac MRI and histology in a female sheep (Charmoise, 2 years old, average weight 50 kg) were conducted at LIRYC in Bordeaux, France. Ischemic scars were created

(A)

(B)
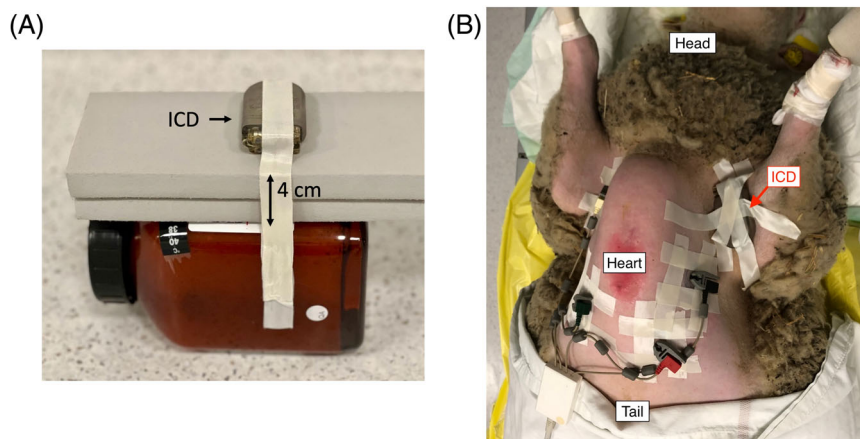
FIGURE 2 (A) Setup of the phantom experiment. The ICD was taped 4 cm away from the side. (B) Setup of the sheep experiment. The ICD was taped on the left shoulder of the sheep, about 10 cm away from the heart. ICD, implantable cardioverter defibrillator.

TABLE 1 Acquisition parameters for conventional and wideband versions of PSIR and BB.

Parameters	Phantom and animal studies		Patient study	
	PSIR	BB	PSIR	BB
FOV (mm)	300 × 225	300 × 225	278–400 × 209–300	278–400 × 209–300
Resolution (mm)	1.4 × 1.4 × 8	1.4 × 1.4 × 8	1.4 × 1.4 × 8	1.4 × 1.4 × 8
TR (ms)	4.8	4.8	4.8	4.8
TE (ms)	2.08	2.08	2.08	2.08
Flip angle (degrees)	15	15	15	15
Sequence	2D GRE	2D GRE	2D GRE	2D GRE
Scan acceleration	GRAPPA ×2	GRAPPA ×2	GRAPPA ×2	GRAPPA ×2
Phase partial Fourier	7/8	7/8	6/8	6/8
Bandwidth (Hz/pixel)	751	751	751	751
Asymmetric echo	Weak	Weak	Weak	Weak
Heartbeat recovery (RR)	1	1	1	1
Nex	4	4	8	8
Number of SA slices	1	1	1	1
Breath-hold	Yes	Yes	Yes	Yes
IR duration (ms)	10.24	10.24	10.24	10.24
Conventional IR BW (kHz)	0.8	0.8	0.8	0.8
Wideband IR BW (kHz)	3.8	3.8	3.8	3.8
TE T_2prep (ms)	n/a	27	n/a	27
Conventional T_2prep BW (kHz)	n/a	1.6	n/a	1.6
Wideband T_2prep BW (kHz)	n/a	5	n/a	5

Abbreviations: BB, black-blood; BW, bandwidth; GRAPPA, generalized autocalibrating partially parallel acquisitions; GRE, gradient echo readout; IR, inversion recovery; n/a, not applicable; Nex, number of averages; PSIR, phase-sensitive inversion recovery; SA, short axis; T_2prep, T_2 preparation; TE, echo time; TR, repetition time.

in the left ventricle by progressively occluding the apical left anterior descending coronary artery and the medial left circumflex coronary artery, deploying an embolization coil pushed by a microcatheter to reduce blood flow.

At 6 weeks post-infarction, cardiac MRI was performed on a 1.5 T system (MAGNETOM Aera, Siemens) with a 32-channel spine coil and an 18-channel cardiac coil, 15 min after injection of gadoterate meglumine

(0.2 mmol/kg of Dotarem), under general anesthesia. Conventional and wideband versions of PSIR and BB LGE imaging were applied with and without ICD. In case of ICD, the ICD (St. Jude Medical, Quadra Assura, model CD3265-40Q) was taped on the left shoulder of the sheep, about 10 cm away from the heart (Figure 2B). Breath-holds were performed via a respirator. Only a single short-axis slice with a noticeable scar was acquired for each sequence. The sequence parameters (Table 1) were the same as in the phantom study, but with different TIs, determined in the same way as for the phantom study.

After MRI, the sheep was euthanized under general anesthesia to perform histology of the heart. The whole heart was fixed in 4% formaldehyde, and a cross-section of the left ventricle scarred tissue was further prepared for histological characterization. Fixed tissues were dehydrated in their cassette with a HistoCore PEARL (Leica Biosystems) overnight. Afterward, the dehydrated tissues were embedded in paraffin using a HistoCore Arcardia C (Leica) and kept at −20°C until use. A thin section of 6 μm was obtained with an RM2255 microtome (Leica) and stained with Masson's trichrome staining using an Autostainer XL workstation (Leica). The obtained section was then scanned with an Axio Scan.Z1 (ZEISS) using a 20× magnification in brightfield.

2.4 | Patient study

All patients were referred for cardiac MRI at the University Hospital CHUV in Lausanne, Switzerland, for clinical purposes independent of this study. All sequences were prospectively tested in six patients, who were not device-dependent, on a 1.5 T system (MAGNETOM Sola, Siemens), using a 32-channel spine coil and an 18-channel cardiac coil. Gadobutrol contrast (Gadovist) was slowly infused (bolus of 0.01 mmol/kg) with a total of 0.2 mmol/kg, ensuring a constant patient-specific TI over time for each of the patient measurements. Devices were interrogated and reprogrammed before and after the MR scan.[4,26] Specific absorption rate (SAR) was maintained below 2 W/kg.

Only a single short-axis slice with a noticeable scar was acquired for each sequence and for every patient. Sequence parameters are reported in Table 1. The number of averages was set to 8. The optimal TIs used for conventional and wideband PSIR were the same and determined with a wideband PSIR TI scout only. Similarly, the optimal TIs used for conventional and wideband BB were the same and determined with a wideband BB TI scout only. Only wideband TI scouts were used to select the optimal TI from a set of images not compromised by ICD hyperintensity artifacts, which themselves could compromise the correct TI selection.

2.5 | Image analysis

2.5.1 | Phantom

By comparing images in the presence of ICD with images in the absence of ICD, hyperintensity artifacts because of the presence of ICD could be distinguished from the phantom signal itself. To assess the performance of the proposed wideband BB sequence in attenuating ICD hyperintensity artifacts, the extent of ICD artifacts (in cm) was measured for each sequence, defined as the maximum spatial extent or the maximal distance from the ICD to the edge of the hyperintensity artifacts. This measurement is illustrated in Figure 3A with a pink arrow. Additionally, the SAR value embedded in the DICOM header was reported for every sequence.

Signal intensity and contrast ratio analyses were performed without the presence of ICD to evaluate the impact of using wideband BB compared with other sequences. As shown in Figure 3A, three phantom vials were used with T_1/T_2 values mimicking "long" post-contrast blood ($T_1/T_2 = 458/189$), "long" post-contrast myocardium ($T_1/T_2 = 562/45$), and "short" post-contrast myocardium ($T_1/T_2 = 300/44$), used to mimic scar tissue in this study. Scar-blood (CR_{blood}^{scar}), scar-myocardium ($CR_{myocardium}^{scar}$), and blood-myocardium ($CR_{myocardium}^{blood}$) contrast ratios were calculated as follows[22]:

$$CR_{blood}^{scar} = \frac{mean(S_{scar}) - mean(S_{blood})}{mean(S_{blood})}$$

$$CR_{myocardium}^{scar} = \frac{mean(S_{scar}) - mean(S_{myocardium})}{mean(S_{myocardium})}$$

$$CR_{myocardium}^{blood} = \frac{mean(S_{blood}) - mean(S_{myocardium})}{mean(S_{myocardium})}$$

where S_{ROI} represents the signal in the region of interest region of interest (ROI).

2.5.2 | Animal

Two expert radiologists scored the subjective image quality using a 4-point Likert scale (1 = non-diagnostic, 2 = less than adequate, 3 = adequate, 4 = excellent) and the overall ICD-artifact severity (hyperintensity artifacts) using a 4-point Likert scale (1 = non-diagnostic with severe ICD artifacts, 2 = less than adequate with large ICD artifacts,
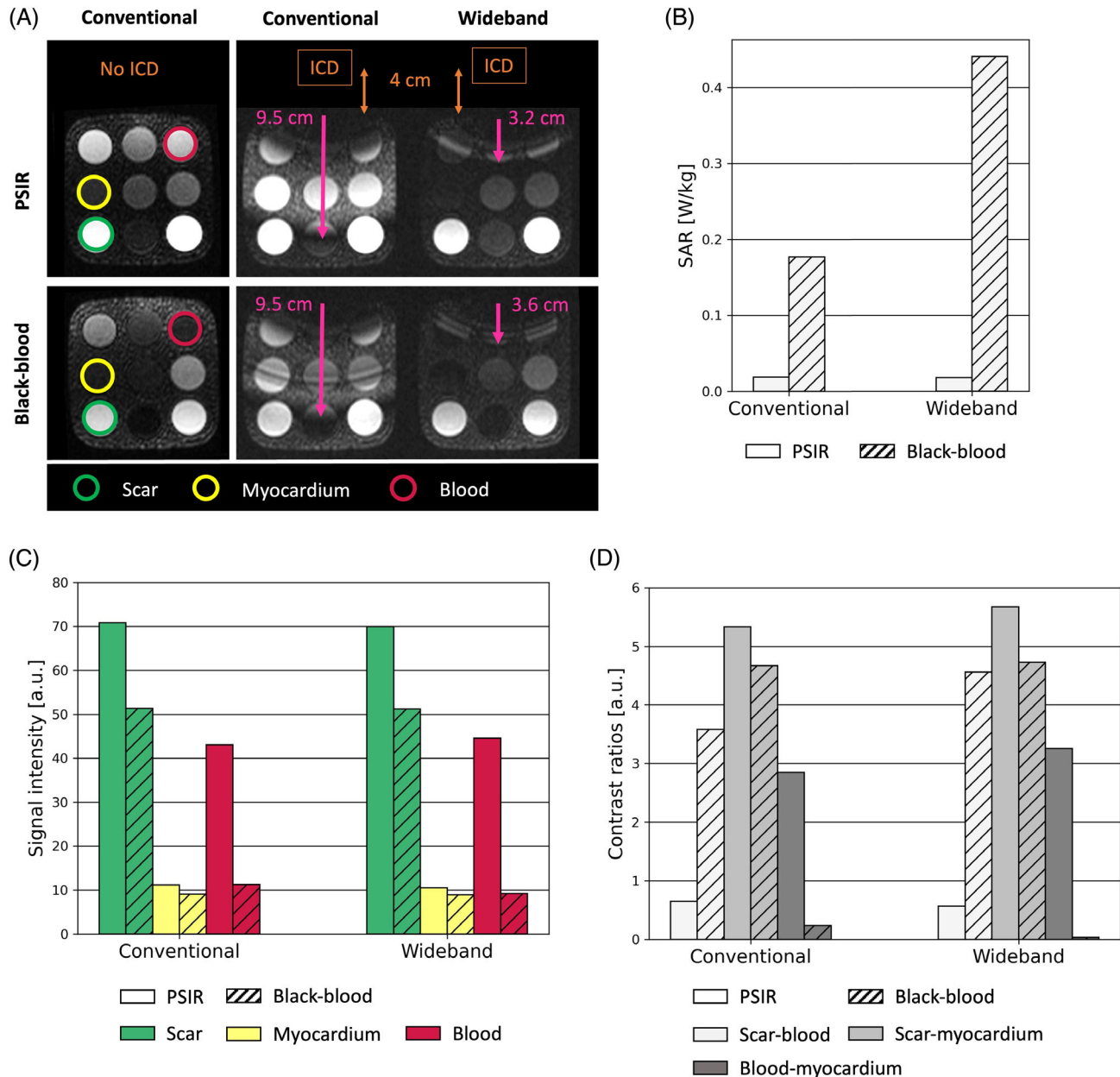
FIGURE 3 T1MES phantom experiment. (A) Results of image acquisition. Top: PSIR images. Bottom: BB images. From the left: first column: measurements without ICD, with conventional PSIR and conventional BB. Second column: measurement with ICD, with conventional PSIR and conventional BB. Third column: measurement with ICD, with wideband PSIR and wideband BB. The ICD was placed 4 cm away from the phantom. The pink arrows show the maximum extent of hyperintensity artifacts in the phantom, regardless of the 4 cm distance between the phantom and the ICD. The SAR for each sequence is shown in (B). The green, yellow, and red circles are the vials mimicking scar, normal myocardium, and blood tissues, respectively, which were used for signal intensity (C) and contrast ratio analyses (D) for each sequence. BB, black-blood; ICD, implantable cardioverter defibrillator; PSIR, phase-sensitive inversion recovery; SAR, specific absorption rate.

3 = adequate with moderate ICD artifacts, 4 = excellent with minimal ICD artifacts), in a blinded manner and in random order. Additionally, the number of scar tissue segments identified in the American Heart Association model[27] was also assessed. The mean and SD between the two readers were reported.

CR_{blood}^{scar}, $CR_{myocardium}^{scar}$, and $CR_{myocardium}^{blood}$ were calculated from images without ICD to assess the impact of wideband BB compared with other sequences on the different contrast ratios. ROIs were manually drawn in part of the myocardium, blood, and scar tissue, in MATLAB (version R2019b, The MathWorks).

Finally, histology of the animal's heart was performed to confirm scar presence and location with respect to MR images.

2.5.3 | Patients

The SAR was reported for every sequence. Additionally, similar to the animal study, three expert radiologists evaluated subjective image quality and the overall severity of ICD artifacts using the 4-point Likert scales defined above, in a blinded manner and in random order. The number of scar tissue segments was also assessed. The mean and SD between the three readers were reported. Furthermore, the quartile range, as well as the mean and SD of all patients, were reported for SAR, image quality, and artifact severity. Finally, statistical analyses were performed using R (R Core Team 4.3.2, 2023) to compare the different sequences in terms of image quality, artifact severity, number of scar segments detected, and SAR. Continuous dependent variables were compared using a two-tailed paired t-test with Bonferroni correction, as all metrics were normally distributed according to a Shapiro–Wilk normality test. Values of $p < 0.05$ indicate statistical significance.

3 | RESULTS

3.1 | Phantom study

Images obtained with each sequence are shown in Figure 3A.

The TI for conventional PSIR (190 ms) obtained with a conventional PSIR TI scout was the same optimal TI for wideband PSIR obtained with a wideband PSIR TI scout. Likewise, the TI for conventional BB (98 ms) obtained with a conventional BB TI scout was the same optimal TI for wideband BB obtained with a wideband BB TI scout.

In the presence of ICD, signal void and hyperintensity artifacts severely degraded conventional PSIR and conventional BB images to an extent of 9.5 cm, with a signal void extent of 2.6 cm. Using wideband versions of both PSIR and BB, the extent of ICD hyperintensity artifacts was reduced to 3.2 cm (66% reduction) and to 3.6 cm (62% reduction), respectively.

The SAR for every sequence is shown in Figure 3B. There was no noticeable change in SAR between conventional PSIR (SAR = 0.018) and wideband PSIR (SAR = 0.018), whereas the SAR of wideband BB (SAR = 0.441) was more than twice that of conventional BB (SAR = 0.177) and more than 24 times that of wideband PSIR.

Signal intensities are shown in Figure 3C. Signal intensities of wideband PSIR (scar, 69.94; blood, 44.59; myocardium, 10.48) were similar to those of conventional PSIR (scar, 70.84; blood, 43.00; myocardium, 11.19), with a near-complete nulling of myocardium signal. Signal intensities of wideband BB (scar, 51.20; blood, 9.21; myocardium, 8.94) were similar to those of conventional BB (scar, 51.33; blood, 11.21; myocardium, 9.06), with a near-complete nulling of normal myocardium and blood signals.

Contrast ratios are shown in Figure 3D. Contrast ratios of conventional PSIR ($CR_{blood}^{scar} = 0.65$, $CR_{myocardium}^{scar} = 5.34$, $CR_{myocardium}^{blood} = 2.85$) and wideband PSIR ($CR_{blood}^{scar} = 0.57$, $CR_{myocardium}^{scar} = 5.68$, $CR_{myocardium}^{blood} = 3.26$) were comparable. Similarly, contrast ratios of conventional BB ($CR_{blood}^{scar} = 3.58$, $CR_{myocardium}^{scar} = 4.67$, $CR_{myocardium}^{blood} = 0.24$) and wideband BB ($CR_{blood}^{scar} = 4.56$, $CR_{myocardium}^{scar} = 4.73$, $CR_{myocardium}^{blood} = 0.03$) were also comparable. Conventional and wideband BB had higher scar-blood and lower blood-myocardium ratios than conventional and wideband PSIR.

3.2 | Animal study

Figure 4A shows images for every sequence with and without ICD. Image quality and artifact severity scores, as well as the number of scarred segments, are presented in Figure 4B–D.

As seen in the phantom study, the TI for conventional PSIR (160 ms) obtained with a conventional PSIR TI scout was the same TI for wideband PSIR obtained with a wideband PSIR TI scout. Similarly, the TI for conventional BB (60 ms) obtained with a conventional BB TI scout was the same TI for wideband BB obtained with a wideband BB TI scout.

In the absence of ICD, image quality (IQ) and artifact severity (AS) scores, and the number of scarred segments (NSS), located in the anterior, lateral, inferior, and septal wall, were the same for conventional and wideband PSIR (IQ = 2.5 ± 0.5, AS = 4.0 ± 0.0, NSS = 4.0 ± 1.0), and the same for conventional and wideband BB (IQ = 3.5 ± 0.5, AS = 4.0 ± 0.0, NSS = 5.0 ± 1.0). Wideband PSIR and BB, therefore, had no impact on image quality compared to their respective conventional version, as observed in the phantom study. Nevertheless, conventional and wideband BB showed a trend toward better image quality and could identify more scar segments than conventional and wideband PSIR.

In the presence of ICD, conventional PSIR images were degraded in the vicinity of the myocardium (IQ = 2.0 ± 0.0, AS = 2.5 ± 0.5), but with preserved ability to identify the
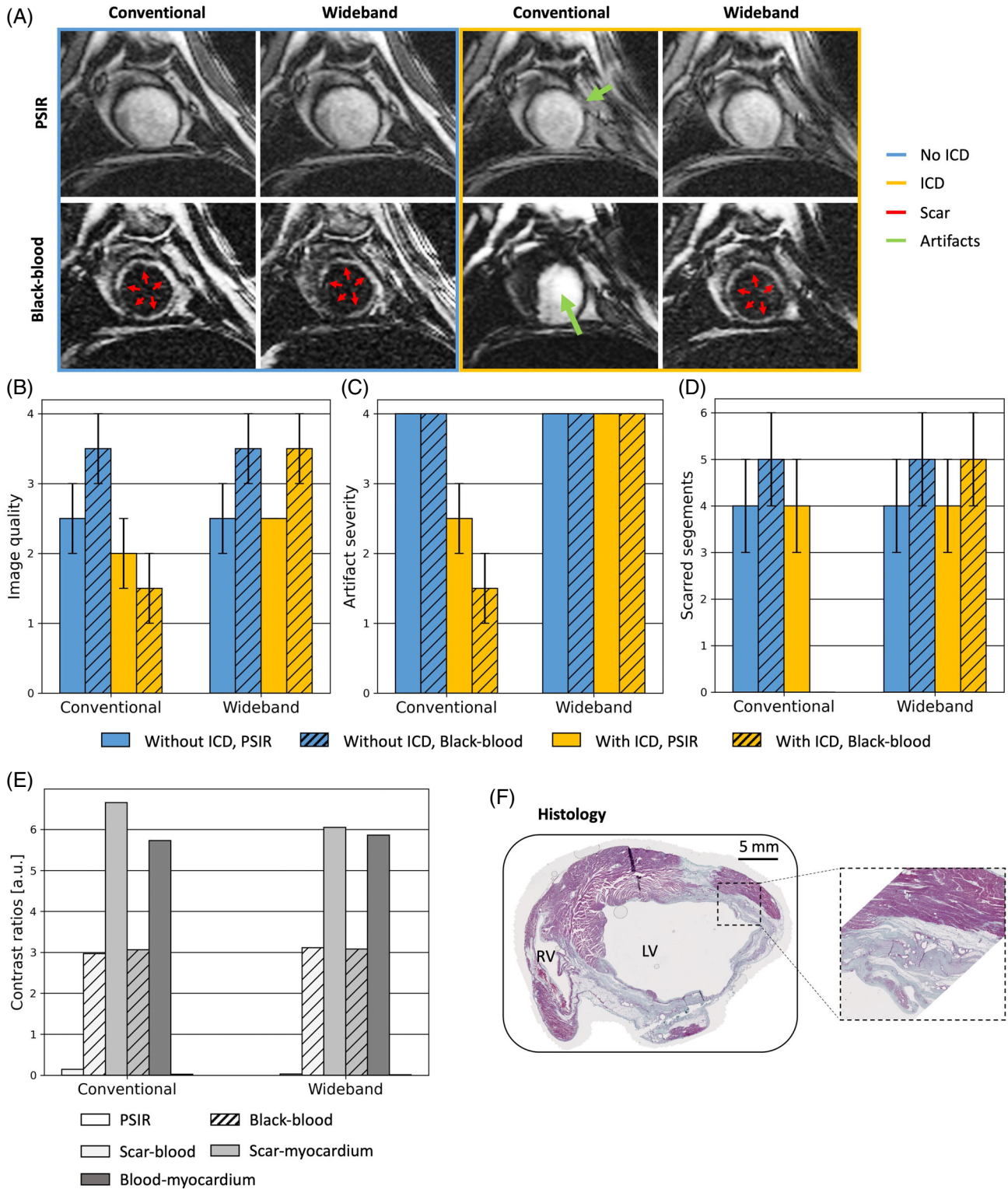
FIGURE 4 Sheep experiment. (A) Top: PSIR LGE images. Bottom: BB LGE images. (B–D) Image quality, artifact severity scores, and detected scarred segments without and with ICD for each sequence. (E) Scar-myocardium, scar-blood, and blood-myocardium contrast ratios for each sequence. (F) Histology: replacement of dense fibro-fatty with surviving myocardial fibers (red/purple = cardiomyocytes; black = nuclei; blue/green = collagen). BB, black-blood; ICD, implantable cardioverter defibrillator; LGE, late gadolinium enhancement; LV, left ventricle; PSIR, phase-sensitive inversion recovery; RV, right ventricle.

infarct (NSS = 4.0 ± 1.0). Wideband PSIR could reduce ICD artifacts (AS = 4.0 ± 0.0), and therefore, improve image quality (IQ = 2.5 ± 0.5, NSS = 4.0 ± 1.0), recovering the results of the case without ICD. Conventional BB images, on the other hand, were severely affected by hyperintensity artifacts over a large portion of the anterior left ventricular wall (AS = 1.5 ± 0.5, IQ = 1.5 ± 0.5), compromising the image interpretation (NSS = 0.0 ± 0.0). Using wideband BB, ICD hyperintensity artifacts were suppressed (AS = 4.0 ± 0.0, IQ = 3.5 ± 0.5), providing images with very good myocardial infarct detection (NSS = 5.0 ± 1.0) and recovering the results of the case without ICD.

Contrast ratios are shown in Figure 4E. Contrast ratios of conventional PSIR ($CR^{scar}_{blood} = 0.14$, $CR^{scar}_{myocardium} = 6.66$, $CR^{blood}_{myocardium} = 5.73$) and wideband PSIR ($CR^{scar}_{blood} = 0.03$, $CR^{scar}_{myocardium} = 6.05$, $CR^{blood}_{myocardium} = 5.86$) were similar, like in the phantom study. Likewise, contrast ratios of conventional BB ($CR^{scar}_{blood} = 2.97$, $CR^{scar}_{myocardium} = 3.06$, $CR^{blood}_{myocardium} = 0.02$) and wideband BB ($CR^{scar}_{blood} = 3.11$, $CR^{scar}_{myocardium} = 3.08$, $CR^{blood}_{myocardium} = 0.01$) were also comparable. Scar-blood contrast was improved with BB compared with PSIR, allowing better scar detection at the scar-blood interface. However, scar-myocardium contrast was reduced with BB compared with PSIR.

Finally, the results of the histology of the sheep are shown in Figure 4F with Masson's trichrome staining of the cross-section of the heart. The histology slice was more basal than the MRI slice. Nevertheless, the histological image showed and confirmed the presence of dense fibro-fatty replacement with diffuse surviving myocardial fibers in the left ventricle.

3.3 | Patient study

Six patients (5 males) with a mean age of 62.0 ± 10.5 years old (range, 45–76 years old) were included in this study. One patient had a pacemaker, and five patients had a transvenous ICD (TV-ICD). Three patients had non-ischemic cardiomyopathy (NICM), and the other three had ischemic cardiomyopathy (ICM). Patients' characteristics are shown in Table 2.

Images obtained with all sequences are shown in Figure 5. SAR, image quality, artifact severity scores, and the number of detected scarred segments are reported in Table 3 and shown in Figure 6. Statistical analyses are reported in Table S1.

Conventional PSIR and BB images were severely degraded by ICD hyperintensity artifacts in four of six (67%) patients (AS$_{PSIR}$ = 2.6 ± 1.1, AS$_{BB}$ = 2.8 ± 0.9), with conventional BB being slightly more impacted

TABLE 2 Patient demographics.

| ID	Gender	Age (y)	Pathology	Device
P1	Male	76	NICM	Pacemaker
P2	Male	45	ICM	TV-ICD
P3	Female	74	ICM	TV-ICD
P4	Male	60	ICM	TV-ICD
P5	Male	58	NICM	TV-ICD
P6	Male	59	NICM	TV-ICD

Abbreviations: ICD, implantable cardioverter defibrillator; ICM, ischemic cardiomyopathy; NICM, non-ischemic cardiomyopathy; TV-ICD, transvenous ICD; y, years old.

($p = 1.000$), as observed in the animal study. This affected image quality (IQ$_{PSIR}$ = 2.3 ± 0.8, IQ$_{BB}$ = 2.4 ± 0.7) and infarct detection (NSS$_{PSIR}$ = 1.6 ± 0.9, NSS$_{BB}$ = 2.3 ± 1.8). The use of wideband PSIR and wideband BB could suppress ICD hyperintensity and, therefore, improve artifact severity by 60% and 65% (AS$_{PSIR}$ = 3.9 ± 0.3, AS$_{BB}$ = 4.0 ± 0.0), respectively, image quality by 42% and 30% (IQ$_{PSIR}$ = 2.9 ± 0.5, IQ$_{BB}$ = 3.2 ± 0.7), respectively, as well as scar detection by 58% and 42% (NSS$_{PSIR}$ = 3.1 ± 2.0, NSS$_{BB}$ = 3.7 ± 1.5), respectively. Overall, more scarred segments could be detected with wideband BB than with wideband PSIR ($p = 0.544$), with similar image quality ($p = 1.000$) and artifact severity ($p = 1.000$), as already seen in the animal study. However, the SAR obtained with wideband BB (SAR = 0.653 ± 0.102) was 24 times higher than the SAR obtained with conventional PSIR (SAR = 0.027 ± 0.007, $p < 0.001$) and wideband PSIR (SAR = 0.027 ± 0.007, $p < 0.001$), and almost three times higher than the SAR obtained with conventional BB (SAR = 0.236 ± 0.047, $p = 0.002$).

In patient 1, pacemaker hyperintensity artifacts were not present on the myocardium in the conventional PSIR (AS = 4.0 ± 0.0) and BB images (AS = 4.0 ± 0.0). Image qualities for both conventional PSIR and BB (IQ$_{PSIR}$ = 2.3 ± 0.6, IQ$_{BB}$ = 2.3 ± 0.6) were not adequate, but scar segments were identified (NSS$_{PSIR}$ = 1.7 ± 0.6, NSS$_{BB}$ = 2.3 ± 1.5). Wideband PSIR and BB did not alter conventional PSIR and BB scores in this patient, but wideband BB identified more scar segments (NSS$_{PSIR}$ = 1.3 ± 0.6, NSS$_{BB}$ = 3.0 ± 1.7).

In patient 2, TV-ICD hyperintensity artifacts were present on the anterior and anterolateral left ventricular wall with conventional PSIR and BB (AS$_{PSIR}$ = 2.3 ± 0.6, AS$_{BB}$ = 2.3 ± 0.6). However, image quality was not very compromised (IQ$_{PSIR}$ = 3.0 ± 1.0, IQ$_{BB}$ = 3.0 ± 0.0), and the anteroseptal scar segments could be identified (NSS$_{PSIR}$ = 2.0 ± 0.0, NSS$_{BB}$ = 2.0 ± 0.0). Wideband PSIR and BB eliminated the hyperintensity artifacts in
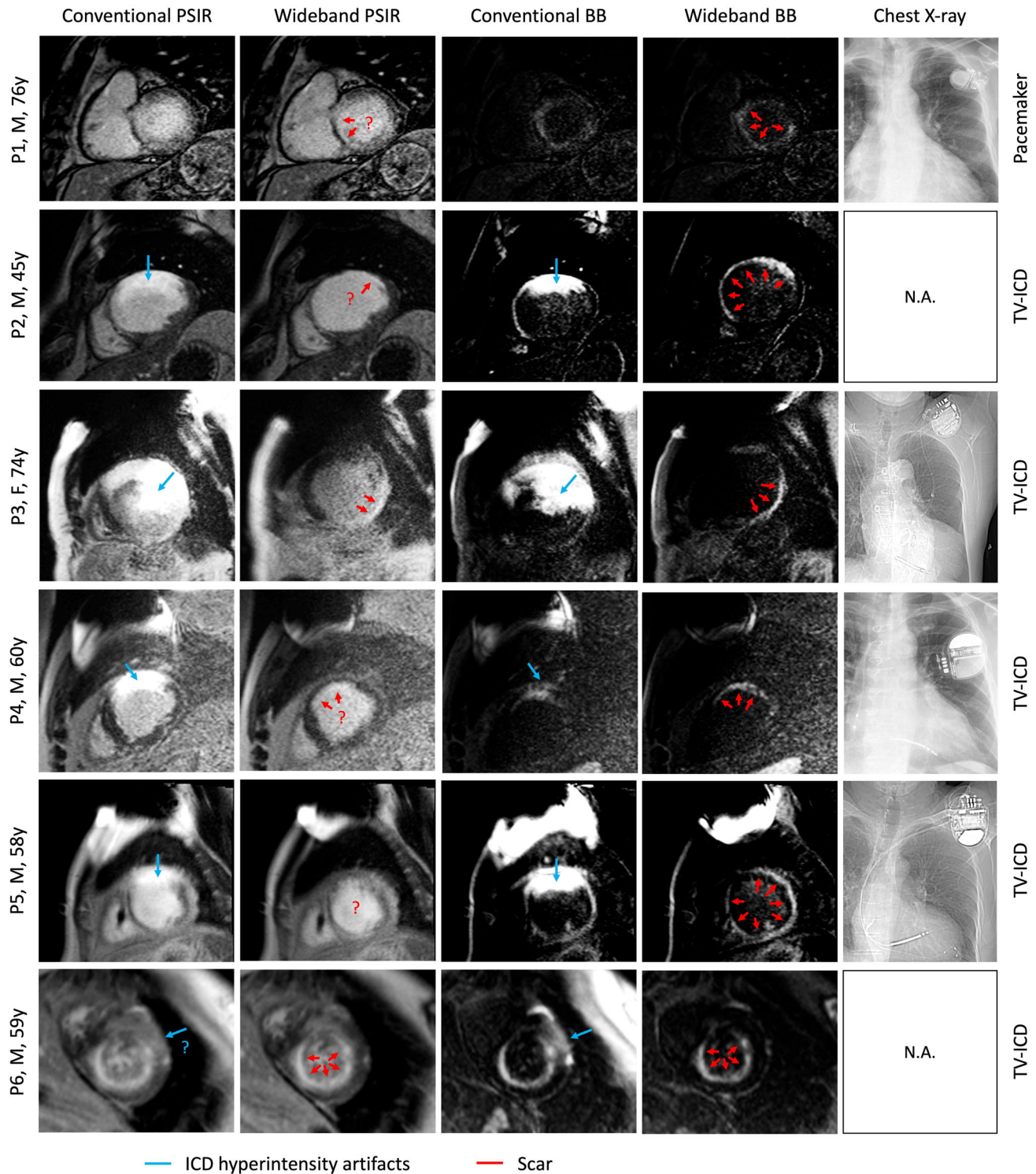
FIGURE 5 Patient study image results. From the left: first column: conventional PSIR LGE with ICD hyperintensity artifacts affecting the myocardium (blue arrow). Second column: wideband PSIR LGE with suppressed ICD artifacts in the myocardium. Third column: conventional BB LGE with ICD hyperintensity artifacts affecting the myocardium (blue arrow). Fourth column: wideband BB LGE with suppressed ICD artifacts in the myocardium. Fifth column: chest X-rays, if available, showing cardiac device position. Blue arrow: ICD hyperintensity artifacts. Red arrow: scar tissue. BB, black-blood; F, female; ICD, implantable cardioverter defibrillator; LGE, late gadolinium enhancement; M, male; N.A., not applicable; PSIR, phase-sensitive inversion recovery; TV-ICD, transvenous ICD; y, years old.

TABLE 3 Analysis of patient images.

Parameter	Sequence	P1	P2	P3	P4	P5	P6	Mean ± SD [Q1 Q3]
SAR	PSIR	0.039	0.023	0.034	0.022	0.026	0.017	0.027 ± 0.007 [0.023 0.032]
	BB	0.291	0.194	0.277	0.252	0.248	0.157	0.236 ± 0.047 [0.207 0.271]
	Wideband PSIR	0.039	0.023	0.034	0.022	0.026	0.017	0.027 ± 0.007 [0.023 0.032]
	Wideband BB	0.767	0.492	0.671	0.586	0.617	0.783	0.653 ± 0.102 [0.594 0.743]
Artifact severity score	PSIR	4.0 ± 0.0	2.3 ± 0.6	1.0 ± 0.0	2.7 ± 0.6	2.0 ± 1.0	3.7 ± 0.6	2.61 ± 1.10 [2.08 3.42]
	BB	4.0 ± 0.0	2.3 ± 0.6	1.3 ± 0.6	3.0 ± 1.0	2.7 ± 1.2	3.3 ± 0.6	2.78 ± 0.91 [2.42 3.25]
	Wideband PSIR	4.0 ± 0.0	4.0 ± 0.0	3.3 ± 0.6	4.0 ± 0.0	4.0 ± 0.0	4.0 ± 0.0	3.89 ± 0.27 [4.00 4.00]
	Wideband BB	4.0 ± 0.0	4.0 ± 0.0	4.0 ± 0.0	4.0 ± 0.0	4.0 ± 0.0	4.0 ± 0.0	4.00 ± 0.00 [4.00 4.00]
Image quality score	PSIR	2.3 ± 0.6	3.0 ± 1.0	1.3 ± 0.6	2.0 ± 1.0	1.7 ± 0.6	3.3 ± 0.6	2.28 ± 0.77 [1.75 2.83]
	BB	2.0 ± 0.0	3.0 ± 0.0	1.3 ± 0.6	2.7 ± 0.6	2.3 ± 0.6	3.3 ± 0.6	2.44 ± 0.72 [2.08 2.92]
	Wideband PSIR	2.3 ± 0.6	3.0 ± 1.0	2.7 ± 0.6	3.3 ± 0.6	2.7 ± 0.6	3.7 ± 0.6	2.94 ± 0.49 [2.67 3.25]
	Wideband BB	2.3 ± 0.6	3.7 ± 0.6	2.7 ± 1.2	3.0 ± 0.0	3.7 ± 0.6	4.0 ± 0.0	3.22 ± 0.66 [2.75 3.67]
Scarred segments	PSIR	1.7 ± 0.6	2.0 ± 0.0	0.0 ± 0.0	0.3 ± 0.6	1.7 ± 2.9	4.0 ± 1.0	1.61 ± 0.90 [0.66 1.92]
	BB	2.3 ± 1.5	2.0 ± 0.0	0.0 ± 0.0	0.7 ± 0.6	4.7 ± 0.6	4.0 ± 1.0	2.28 ± 1.80 [1.00 3.58]
	Wideband PSIR	1.3 ± 0.6	3.7 ± 0.6	2.3 ± 0.6	1.0 ± 0.0	6.0 ± 0.0	4.0 ± 1.0	3.06 ± 2.04 [1.58 3.92]
	Wideband BB	3.0 ± 1.7	3.7 ± 0.6	3.3 ± 1.2	2.0 ± 0.0	6.0 ± 0.0	4.0 ± 1.0	3.67 ± 1.48 [3.08 3.92]

Note: SAR, artifact severity, and image quality scores, as well as the number of detected scarred segments, are reported for each patient. Scores are presented as the mean and SD of the assessments made by the three expert radiologists. The last column on the right indicates the mean and SD for the entire population, along with the first and third quartiles.

Abbreviations: BB, black-blood; PSIR, phase-sensitive inversion recovery; Q1, first quartile; Q3, third quartile; SAR, specific absorption rate.

the left ventricle ($AS_{PSIR} = 4.0 \pm 0.0$, $AS_{BB} = 4.0 \pm 0.0$, $IQ_{PSIR} = 3.0 \pm 1.0$, $IQ_{BB} = 3.7 \pm 0.6$), revealing the anterior and anterolateral scar segments ($NSS_{PSIR} = 3.7 \pm 0.6$, $NSS_{BB} = 3.7 \pm 0.6$).

In patient 3, TV-ICD hyperintensity artifacts affected almost the entire left ventricle using conventional PSIR and BB ($AS_{PSIR} = 1.0 \pm 0.0$, $AS_{BB} = 1.3 \pm 0.6$), heavily affecting the image quality ($IQ_{PSIR} = 1.3 \pm 0.6$, $IQ_{BB} = 1.3 \pm 0.6$). Many scar tissues could not be identified on these images, although a scar in the inferior wall could be detected ($NSS_{PSIR} = 0.0 \pm 0.0$, $NSS_{BB} = 0.0 \pm 0.0$). Wideband PSIR and BB eliminated ICD hyperintensity artifacts ($AS_{PSIR} = 4.0 \pm 0.0$, $AS_{BB} = 4.0 \pm 0.0$), making the image interpretation possible ($IQ_{PSIR} = 3.0 \pm 0.0$, $IQ_{BB} = 3.0 \pm 1.0$), with the detection of scar segments in the inferolateral wall ($NSS_{PSIR} = 2.3 \pm 0.6$), as well as in the anterolateral wall with BB only ($NSS_{BB} = 3.3 \pm 1.2$).

In patient 4, TV-ICD hyperintensity artifacts were prominent on the anterior left ventricular wall using conventional PSIR ($AS_{PSIR} = 2.7 \pm 0.6$), severely compromising the image interpretability ($IQ_{PSIR} = 2.0 \pm 1.0$) and hiding an eventual anterior scar ($NSS_{PSIR} = 0.3 \pm 0.6$). Wideband PSIR could subsequently improve the image interpretability ($AS_{PSIR} = 4.0 \pm 0.0$, $IQ_{PSIR} = 3.3 \pm 0.6$),

and the anterior scar could be successfully resolved ($NSS_{PSIR} = 1.0 \pm 0.0$). ICD hyperintensity artifacts were, on the other hand, minimal with conventional BB ($AS_{BB} = 3.0 \pm 1.0$, $IQ_{BB} = 2.7 \pm 0.6$), and the anterior scar could be identified ($NSS_{BB} = 0.7 \pm 0.6$). Wideband BB suppressed the minimal artifacts ($AS_{BB} = 4.0 \pm 0.0$, $IQ_{BB} = 3.0 \pm 0.0$), revealing an anterolateral scar ($NSS_{BB} = 2.0 \pm 0.0$).

In patient 5, large TV-ICD hyperintensity artifacts on the anterior and anterolateral wall with conventional PSIR and BB images ($AS_{PSIR} = 2.0 \pm 1.0$, $AS_{BB} = 2.7 \pm 1.2$) degraded image quality ($IQ_{PSIR} = 1.7 \pm 0.6$, $IQ_{BB} = 2.7 \pm 0.6$), hiding eventual scars. Nevertheless, the anteroseptal and inferoseptal scars could be well identified ($NSS_{PSIR} = 1.7 \pm 2.9$), as well as the inferior, inferolateral and anterolateral scars with BB ($NSS_{BB} = 4.7 \pm 0.6$). Wideband PSIR and BB could identify all scar segments ($NSS_{PSIR} = 6.0 \pm 0.0$, $NSS_{BB} = 6.0 \pm 0.0$), achieved by suppressing hyperintensity artifacts ($AS_{PSIR} = 4.0 \pm 0.0$, $AS_{BB} = 4.0 \pm 0.0$) and improving image quality ($IQ_{PSIR} = 2.7 \pm 0.6$, $IQ_{BB} = 3.7 \pm 0.6$).

Finally, in patient 6, TV-ICD hyperintensity artifacts were minimal on the selected apical slice using conventional PSIR and ($AS_{PSIR} = 3.7 \pm 0.6$, $AS_{BB} = 3.3 \pm 0.6$),
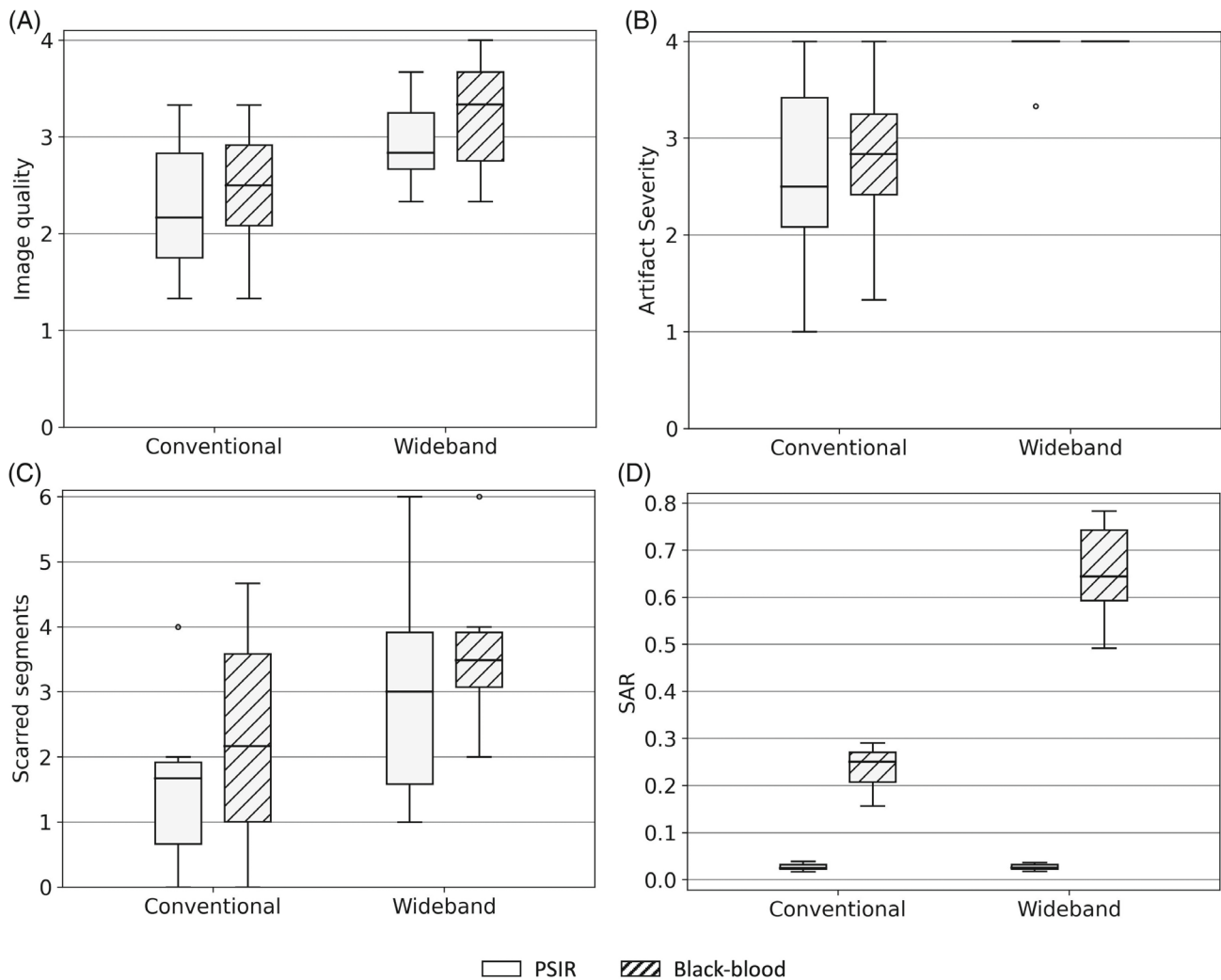
FIGURE 6 Quantitative results of the patient study. (A) Image quality, (B) artifact severity, (C) detected scarred segments, and (D) SAR for the entire patient population and for each sequence. BB, black-blood; PSIR, phase-sensitive inversion recovery.

because of the greater distance between the ICD and the apex than between the ICD and the base. Therefore, image quality ($IQ_{PSIR} = 3.3 \pm 0.6$, $IQ_{BB} = 3.3 \pm 0.6$) and image interpretability were not affected, and inferior, lateral, and anterior scars could be well discerned ($NSS_{PSIR} = 4.0 \pm 1.0$, $NSS_{BB} = 4.0 \pm 1.0$). In this case, wideband PSIR and BB did not considerably improve artifact severity ($AS_{PSIR} = 4.0 \pm 0.0$, $AS_{BB} = 4.0 \pm 0.0$) and image quality scores ($IQ_{PSIR} = 3.7 \pm 0.6$, $IQ_{BB} = 4.0 \pm 0.0$), and the same number of scar segments were detected ($NSS_{PSIR} = 4.0 \pm 1.0$, $NSS_{BB} = 4.0 \pm 1.0$).

4 | DISCUSSION AND CONCLUSION

Assessment of myocardial scars in ICD patients is essential to better understand the underlying structural abnormalities of the heart. To suppress ICD hyperintensity artifacts, wideband PSIR has been developed[11] and tested in several studies.[23,28–31] Despite the artifact reduction, wideband PSIR LGE suffers from poor contrast at the scar-blood interface, challenging the depiction of small and subendocardial scars. Therefore, a 2D breath-hold single-shot ECG-triggered GRE wideband BB LGE sequence was implemented to suppress ICD artifacts and to improve scar detection.

Conventional PSIR and conventional BB consisted of an IR bandwidth of 0.8 kHz and a T_2prep refocusing bandwidth of 1.6 kHz for BB. To reduce ICD hyperintensity artifacts in the myocardium from the non-properly inverted spins, the IR bandwidth was increased to 3.8 kHz[11] in wideband PSIR and wideband BB. To further decrease hyperintensity artifacts because of the strong off-resonance in the wideband BB sequence, the T_2prep refocusing bandwidth was increased to 5.0 kHz.

RF excitation pulses for readout were not modified in this study, but the ICD artifacts might also be linked with the RF excitation pulses used for imaging.[23] Altered precession frequencies in the vicinity of the devices can give rise to artifacts during signal-readout. In this study, the slice-selective RF excitation pulse was a sinc pulse with a bandwidth of 3.7 kHz. According to the results obtained with the phantom, the RF excitation pulse was not modified, because the images obtained using wideband PSIR as well as wideband BB were not affected by severe residual ICD artifacts. Furthermore, the clinical conventional slice thickness of 8 mm was used. As described in a previous study,[23] the distortion of the slice profile is proportional to the slice thickness and inversely proportional to the RF bandwidth. The slab distortion in a region where the resonance offset is 3 kHz (~7 cm from ICD[11]) using a slice thickness of 8 mm and an RF excitation pulse with a bandwidth of 3.7 kHz is 6.4 mm. However, to obtain images with high signal, particularly for BB imaging, the slice thickness was not reduced.

In the implemented BB sequences, the time delay between the IR and T_2prep pulses was set to zero. Although this time delay is a crucial parameter that affects the overall contrast and efficiency of the BB preparation,[16] the decision to set the delay to zero was justified with the objective of facilitating clinical applicability and faster image acquisition. The design of this sequence was intended to simplify the workflow for clinical technicians, improve user-friendliness, and facilitate integration into clinical routine protocols.

Conventional and wideband versions of both PSIR and BB were tested in a phantom and an animal with and without an ICD, and were prospectively applied in six patients, one with a pacemaker and five with ICDs.

In the absence of ICD, the phantom and animal studies showed that contrast ratios were not affected by increasing spectral bandwidths in wideband PSIR and wideband BB. Contrast ratios were, therefore, similar between conventional and wideband PSIR, and similar between conventional and wideband BB. Compared with conventional and wideband PSIR, the simultaneous nulling of blood and healthy myocardial signals using conventional and wideband BB resulted in a substantial reduction in the blood signal and, consequently, a significant improvement in the scar-blood contrast ratio. However, because of T_2 signal weighting[13] in BB imaging, scar signal was slightly reduced compared to PSIR imaging, resulting in a reduced scar-myocardium contrast ratio. This loss of signal using BB imaging may be compensated for by signal averaging. Furthermore, the difference in scar-myocardium contrast between wideband PSIR and wideband BB imaging was greater in the animal than in the phantom, likely associated with different relaxation times between the two

studies, and therefore, a difference in the optimal TIs chosen. Finally, and similarly to the contrast ratios, the animal study also showed that the artifact severity, image quality, and number of scarred segments were the same for conventional and wideband PSIR, and the same for conventional and wideband BB. However, conventional BB and wideband BB showed a trend toward better image quality and scar detection than conventional and wideband PSIR, because of a superior scar-blood contrast ratio.

In the presence of ICD, conventional PSIR and conventional BB were similarly affected by ICD hyperintensity artifacts in the phantom study. Wideband PSIR and wideband BB considerably reduced the hyperintensity artifacts compared to conventional PSIR (62%) and conventional BB (66%), respectively. In the animal study, conventional BB was severely affected by hyperintensity artifacts, impacting scar detection, and resulting in low image quality and artifact severity. Wideband BB successfully suppressed hyperintensity artifacts in the myocardium, improving image quality and revealing all scar segments. It was also shown that wideband BB recovered image quality and artifact severity scores, and the number of scar segments as in the case without ICD. Compared to wideband PSIR, it was shown that wideband BB could identify more scar segments and with a trend toward better image quality.

As in the animal study, conventional PSIR and conventional BB were severely affected by hyperintensity artifacts because of ICD in four of six patients, compromising their image interpretability. In two of six patients, the myocardium was not affected by the artifacts induced by the implantable cardiac devices. One of these two patients had a pacemaker, and, because of its smaller size than that of an ICD, it has already been shown in previous studies[9,32] that pacemakers generally do not produce hyperintensity artifacts in the myocardium. For the other patient with an ICD, an apical slice was selected for measurement. Because the distance between the apex and the ICD was relatively large, this patient's myocardium was not obscured by hyperintensity artifacts. Overall, compared with conventional PSIR and conventional BB, wideband PSIR and wideband BB successfully removed all myocardial ICD hyperintensity artifacts in all patients, improving artifact severity by 60% and 65%, respectively, image quality by 42% and 30%, respectively, and scar detection by 58% and 48%, respectively. Wideband BB was also shown to detect more scar segments with a trend toward higher image quality than wideband PSIR.

Results from the animal and patient studies have shown that wideband BB LGE imaging was more sensitive in detecting myocardial scars than reference wideband PSIR LGE. This may allow for a more precise and reliable assessment of myocardial scars, which would have an

impact on the diagnosis and treatment of ICD patients. However, the wideband BB sequence was associated with a considerable increase in SAR, almost three times that of the conventional BB sequence and 24 times that of the conventional and wideband PSIR sequences. The increase in SAR of the wideband BB sequence compared with the wideband PSIR sequence is because of the four additional pulses in the T_2prep of the BB sequence. Additionally, the SAR of wideband BB was much higher than that of conventional BB, because of the increased B_1 amplitudes in the IR as well as in the two T_2prep refocusing pulses as a result of their increased spectral bandwidths. Nevertheless, the SAR was always kept below the limit of 2 W/kg.

Finally, the histology of the sheep's heart revealed the presence of scar tissues in the inferoseptal, inferior, inferolateral, anterolateral, and anterior regions of the left ventricle. Although the histological section of the animal's cardiac tissue was more basal than the corresponding MRI slice, the histological results nevertheless confirmed the presence of scar tissue in these regions. Despite this slice mis-registration, because of the large extent of the infarct, histology was still able to show scar segment locations similar to those on MRI, apart from the anteroseptal scar segment. Additionally, it also showed that no new artifacts were created with wideband BB. These findings demonstrated the validity of the proposed 2D wideband BB LGE sequence. Last, the comparison between histology and MRI also showed the limitations and difficulties of BB imaging in assessing scar transmurality and localization in the myocardial wall.

Wideband BB imaging has promising clinical implications. Among the various applications of wideband BB imaging is its potential utility in identifying ablation targets for catheter-guided ablation procedures, in assessing myocardial viability, and in optimizing ICD programming decisions to improve device efficiency and reduce unnecessary interventions. Adoption of wideband BB imaging into clinical practice for ICD patients will require further validation through clinical studies, in terms of reliability, reproducibility, and overall clinical impact.

4.1 | Limitations and future work

This study had several limitations. One was the small size of the patient and animal samples. Additionally, because of the limited time available for patient and animal acquisitions, only one slice per sequence was acquired. Further whole-heart clinical studies, multicenter studies, including a larger number of animals and patients with chronic and acute myocardial lesions, with extensive statistical analysis of the different metrics between the different sequences, are now warranted to further validate the proposed technique.

One of the main limitations of this study was the lack of anatomical information obtained using conventional or wideband BB LGE compared with conventional or wideband PSIR LGE. Despite the improvement in contrast at the scar-blood interface with conventional and wideband BB, and the resultant improvement in scar detection, the simultaneous nulling of blood and healthy myocardial signals nevertheless limited the localization of myocardial infarction, challenging the characterization of scar transmurality. Gray-blood imaging,[33] on the one hand, has been proposed to improve scar-blood contrast compared to PSIR imaging, while maintaining anatomical information. Moreover, it has been suggested that bright- and BB imaging can be combined in the same sequence,[34] providing anatomical information with bright-blood images, and enhancing scar detection with BB images, particularly for small and subendocardial lesions, therefore, facilitating the assessment of potential myocardial injury. In the future, wideband BB imaging could, therefore, be combined with wideband bright-blood imaging in a single sequence to improve scar detection and localization, with attenuation of ICD artifacts.

Finally, further improvements to the proposed 2D wideband BB sequence could be implemented. Different wideband T_2prep modules and their impact on artifact reduction, scar detection, and SAR could be investigated. Additionally, a 3D wideband BB sequence would be of particular interest for better detection of small scars that could be missed with 2D whole-heart coverage, as well as for 3D modeling of myocardial scars to facilitate catheter ablation. Another improvement could be the implementation of a free-breathing acquisition to reduce slice mismatch using co-registration, alleviate the burden of apnea on patients, and reduce acquisition time.

5 | CONCLUSION

In conclusion, the proposed 2D breath-hold single-shot ECG-triggered GRE wideband BB LGE imaging technique was able to reduce ICD hyperintensity artifacts while improving scar detection. This may make it a promising technique, especially if combined with wideband bright-blood LGE,[34] for scar assessment in ICD patients, particularly for small and subendocardial infarctions, where conventional and wideband PSIR LGE suffer from poor scar-blood contrast.

CONFLICT OF INTEREST STATEMENT

ORCID
Pauline Gut https://orcid.org/0000-0003-0554-4974
Hubert Cochet https://orcid.org/0000-0001-7772-5331
Guido Caluori https://orcid.org/0000-0003-2725-8768
Marion Constantin https://orcid.org/0009-0000-3085-593X
Konstantinos Vlachos https://orcid.org/0000-0002-7543-3236
Soumaya Sridi https://orcid.org/0000-0002-0307-1758
Panagiotis Antiochos https://orcid.org/0000-0001-8466-7360
Jürg Schwitter https://orcid.org/0000-0002-9966-6149
Ambra Masi https://orcid.org/0000-0003-0535-1187
Frederic Sacher https://orcid.org/0000-0003-4647-8694
Pierre Jaïs https://orcid.org/0000-0002-4700-7811
Matthias Stuber https://orcid.org/0000-0001-9843-2028
Aurélien Bustin https://orcid.org/0000-0002-2845-8617

TWITTER
Aurélien Bustin AurelienBustin

REFERENCES
1. Tsao CW, Aday AW, Almarzooq ZI, et al. Heart disease and stroke statistics-2022 update: a report from the American Heart Association. *Circulation*. 2022;145:E153-E639. doi:10.1161/CIR.0000000000001052
2. Jean-Philippe E, Lerner I, Valentin E, et al. Incidence of sudden cardiac death in the European Union. *J Am Coll Cardiol*. 2022;79:1818-1827. doi:10.1016/J.JACC.2022.02.041
3. Kusumoto FM, Schoenfeld MH, Wilkoff BL, et al. 2017 HRS expert consensus statement on cardiovascular implantable electronic device lead management and extraction. *Heart Rhythm*. 2017;14:e503-e551. doi:10.1016/J.HRTHM.2017.09.001
4. Nazarian S, Roguin A, Zviman MM, et al. Clinical utility and safety of a protocol for noncardiac and cardiac magnetic resonance imaging of patients with permanent pacemakers and implantable-cardioverter defibrillators at 1.5 tesla. *Circulation*. 2006;114:1277-1284. doi:10.1161/CIRCULATIONAHA.105.607655
5. Nazarian S, Hansford R, Roguin A, et al. A prospective evaluation of a protocol for magnetic resonance imaging of patients with implanted cardiac devices. *Ann Intern Med*. 2011;155:415-424. doi:10.7326/0003-4819-155-7-201110040-00004
6. Cohen JD, Costa HS, Russo RJ. Determining the risks of magnetic resonance imaging at 1.5 tesla for patients with pacemakers and implantable cardioverter defibrillators. *Am J Cardiol*. 2012;110:1631-1636. doi:10.1016/j.amjcard.2012.07.030
7. Roguin A, Schwitter J, Vahlhaus C, et al. Magnetic resonance imaging in individuals with cardiovascular implantable electronic devices. *Europace*. 2008;10:336-346. doi:10.1093/europace/eun021
8. Roguin A, Donahue JK, Bomma CS, Bluemke DA, Halperin HR. Cardiac magnetic resonance imaging in a patient with implantable cardioverter-defibrillator. *Pacing Clin Electrophysiol*. 2005;28:336-338. doi:10.1111/J.1540-8159.2005.40032.X
9. Sasaki T, Hansford R, Zviman MM, et al. Quantitative assessment of artifacts on cardiac magnetic resonance imaging of patients with pacemakers and implantable cardioverter defibrillators. *Circ Cardiovasc Imaging*. 2011;4:662-670. doi:10.1161/CIRCIMAGING.111.965764
10. Dickfeld T, Tian J, Ahmad G, et al. MRI-guided ventricular tachycardia ablation integration of late gadolinium-enhanced 3D scar in patients with implantable cardioverter-defibrillators. *Circ Arrhythm Electrophysiol*. 2011;4:172-184. doi:10.1161/CIRCEP.110.958744/FORMAT/EPUB
11. Rashid S, Rapacchi S, Vaseghi M, et al. Improved late gadolinium enhancement MR imaging for patients with implanted cardiac devices. 2014;270:269-274. doi:10.1148/radiol.13130942
12. Foo TKF, Wolff SD, Gupta SN, Kraitchman DL. Enhanced viability imaging: improved contrast in myocardial delayed enhancement using dual inversion time subtraction. *Magn Reson Med*. 2005;53:1484-1489. doi:10.1002/mrm.20515
13. Kellman P, Chung YC, Simonetti OP, McVeigh ER, Arai AE. Multicontrast delayed enhancement provides improved contrast between myocardial infarction and blood pool. *J Magn Reson Imaging*. 2005;22:605-613. doi:10.1002/JMRI.20426
14. Nezafat R, Stuber M, Ouwerkerk R, Gharib AM, Desai MY, Pettigrew RI. B1-insensitive T_2 preparation for improved coronary magnetic resonance angiography at 3 T. *Magn Reson Med*. 2006;55:858-864. doi:10.1002/mrm.20835
15. Basha T, Roujol S, Kissinger KV, Goddu B, Manning WJ, Nezafat R. Black blood late gadolinium enhancement using combined T_2 magnetization preparation and inversion recovery. *J Cardiovasc Magn Reson*. 2015;17:1-2. doi:10.1186/1532-429X-17-S1-O14
16. Kellman P, Xue H, Olivieri LJ, et al. Dark blood late enhancement imaging. *J Cardiovasc Magn Reson*. 2016;18:1-11. doi:10.1186/S12968-016-0297-3/FIGURES/10
17. Kim HW, Rehwald WG, Wendell DC, et al. Flow-independent dark-blood delayed enhancement (fiddle): validation of a novel black blood technique for the diagnosis of myocardial infarction. *J Cardiovasc Magn Reson*. 2016;18:1-3. doi:10.1186/1532-429X-18-S1-O55/TABLES/1
18. Muscogiuri G, Rehwald WG, Schoepf UJ, et al. T(Rho) and magnetization transfer and INvErsion recovery (TRAMINER)-prepared imaging: a novel contrast-enhanced flow-independent dark-blood technique for the evaluation of myocardial late gadolinium enhancement in patients with myocardial infarction. *J Magn Reson Imaging*. 2017;45:1429-1437. doi:10.1002/jmri.25498
19. Basha TA, Tang MC, Tsao C, et al. Improved dark blood late gadolinium enhancement (DB-LGE) imaging using

an optimized joint inversion preparation and T_2 magnetization preparation. *Magn Reson Med.* 2018;79:351-360. doi:10.1002/mrm.26692

20. Liu CY, Wieben O, Brittain JH, Reeder SB. Improved delayed enhanced myocardial imaging with T_2-prep inversion recovery magnetization preparation. *J Magn Reson Imaging.* 2008;28:1280-1286. doi:10.1002/jmri.21560

21. Kellman P, Olivieri L, Grant E, et al. Dark blood late gadolinium enhancement improves conspicuity of ablation lesions. *J Cardiovasc Magn Reson.* 2016;18:1-2. doi:10.1186/1532-429X-18-S1-P211

22. Sridi S, Nuñez-Garcia M, Sermesant M, et al. Improved myocardial scar visualization with fast free-breathing motion-compensated black-blood T_1-rho-prepared late gadolinium enhancement MRI. *Diagn Interv Imaging.* 2022;103:607-617. doi:10.1016/J.DIII.2022.07.003

23. Rashid S, Rapacchi S, Shivkumar K, Plotnik A, Finn JP, Hu P. Modified wideband three-dimensional late gadolinium enhancement MRI for patients with implantable cardiac devices HHS public access. *Magn Reson Med.* 2016;75:572-584. doi:10.1002/mrm.25601

24. Captur G, Gatehouse P, Keenan KE, et al. A medical device-grade T_1 and ECV phantom for global T_1 mapping quality assurance – the T_1 mapping and ECV standardization in cardiovascular magnetic resonance (T1MES) program. *J Cardiovasc Magn Reson.* 2016;18:1-20. doi:10.1186/S12968-016-0280-Z/TABLES/4

25. Captur G, Bhandari A, Brühl R, et al. T_1 mapping performance and measurement repeatability: results from the multi-national T_1 mapping standardization phantom program (T1MES). *J Cardiovasc Magn Reson.* 2020;22:31. doi:10.1186/s12968-020-00613-3

26. Nazarian S, Halperin HR. How to perform magnetic resonance imaging on patients with implantable cardiac arrhythmia devices. *Heart Rhythm.* 2009;6:138-143. doi:10.1016/j.hrthm.2008.10.021

27. Cerqueira MD, Weissman NJ, Dilsizian V, et al. Standardized myocardial sementation and nomenclature for tomographic imaging of the heart: a statement for healthcare professionals from the Cardiac Imaging Committee of the Council on Clinical Cardiology of the American Heart Association. *Circulation.* 2002;105:539-542. doi:10.1161/HC0402.102975/FORMAT/EPUB

28. Ranjan R, McGann CJ, Jeong EK, et al. Wideband late gadolinium enhanced magnetic resonance imaging for imaging myocardial scar without image artefacts induced by implantable cardioverter-defibrillator: a feasibility study at 3 T. *Europace.* 2015;17:483-488. doi:10.1093/EUROPACE/EUU263

29. Schwartz SM, Pathrose A, Serhal AM, et al. Evaluation of image quality of wideband single-shot late gadolinium-enhancement MRI in patients with a cardiac implantable electronic device. *J Cardiovasc Electrophysiol.* 2021;32:138-147. doi:10.1111/JCE.14798

30. Hong K, Jeong EK, Wall TS, Drakos SG, Kim D. Wideband arrhythmia-insensitive-rapid (AIR) pulse sequence for cardiac T_1 mapping without image artifacts induced by an implantable-cardioverter-defibrillator. *Magn Reson Med.* 2015;74:336-345. doi:10.1002/mrm.25712

31. Shao J, Rashid S, Renella P, Nguyen KL, Hu P. Myocardial T_1 mapping for patients with implanted cardiac devices using wideband inversion recovery spoiled gradient echo readout. *Magn Reson Med.* 2017;77:1495-1504. doi:10.1002/mrm.26223

32. Kaasalainen T, Kivistö S, Holmström M, et al. Cardiac MRI in patients with cardiac pacemakers: practical methods for reducing susceptibility artifacts and optimizing image quality. *Acta Radiol.* 2016;57:178-187. doi:10.1177/0284185115574873

33. Holtackers RJ, Van De Heyning CM, Chiribiri A, Wildberger JE, Botnar RM, Kooi ME. Dark-blood late gadolinium enhancement cardiovascular magnetic resonance for improved detection of subendocardial scar: a review of current techniques. *J Cardiovasc Magn Reson.* 2021;23:1-18. doi:10.1186/S12968-021-00777-6/TABLES/2

34. Bustin A, Sridi S, Kamakura T, Jais P, Stuber M, Cochet H. Free-breathing joint bright- and black-blood cardiovascular magnetic resonance imaging for the improved visualization of ablation-related radiofrequency lesions in the left ventricle. *Europace.* 2022;24:euac053-594. doi:10.1093/EUROPACE/EUAC053.594

SUPPORTING INFORMATION

Additional supporting information may be found in the online version of the article at the publisher's website.

Table S1. Statistical analysis between the different sequences in patients.

How to cite this article: Gut P, Cochet H, Caluori G, et al. Wideband black-blood late gadolinium enhancement imaging for improved myocardial scar assessment in patients with cardiac implantable electronic devices. *Magn Reson Med.* 2024;92:1851-1866. doi: 10.1002/mrm.30162